# Ghost ray reduction and early results from the third FOXSI sounding rocket flight

Sophie Musset<sup>a</sup>, Juan Camilo Buitrago-Casas<sup>b</sup>, Lindsay Glesener<sup>a</sup>, Stephen Bongiorno<sup>c</sup>, Sasha Courtade<sup>b</sup>, P. S. Athiray<sup>a,c</sup>, Juliana Vievering<sup>a</sup>, Shin-nosuke Ishikawa<sup>d</sup>, Noriyuki Narukage<sup>e</sup>, Kento Furukawa<sup>f</sup>, Daniel Ryan<sup>g</sup>, Gregory Dalton<sup>b</sup>, Zoe Turin<sup>j,l</sup>, Lance Davis<sup>a,k</sup>, Tadayuki Takahashi<sup>f</sup>, Shin Watanabe<sup>h</sup>, Ikuyuki Mitsuishi<sup>d</sup>, Kouichi Hagino<sup>i</sup>, Tomoko Kawate<sup>h</sup>, Paul Turin<sup>b</sup>, Steven Christe<sup>g</sup>, Brian Ramsey<sup>c</sup>, and Säm Krucker<sup>b</sup>

<sup>a</sup>University of Minnesota, 116 Church St SE, Minneapolis, USA

<sup>b</sup>University of California, Berkeley, USA

<sup>c</sup>NASA Marshall Space Flight Center, USA

<sup>d</sup>Nagoya University, Japan

<sup>e</sup>National Astronomical Observatory of Japan, Japan

<sup>e</sup>National Astronomical Observatory of Japan, Japan

<sup>f</sup>Kavli Institute for the Physics and Mathematics of the Universe (WPI), The University of Tokyo, Japan

<sup>g</sup>NASA Goddard Space Flight Center, USA

<sup>h</sup>Institute of Space and Astronautical Science, Japan Aerospace Exploration Agency, Japan 
<sup>i</sup>Tokyo University of Science, Japan 
<sup>j</sup>University of Colorado, USA 
<sup>k</sup>University of New Hampshire, USA 
<sup>l</sup>Georgia Institute of Technology, USA

#### ABSTRACT

The Focusing Optics X-ray Solar Imager (FOXSI) sounding rocket experiment demonstrates the technique of focusing hard X-ray (HXR) optics for the study of fundamental questions about the high-energy Sun. Solar HXRs provide one of the most direct diagnostics of accelerated electrons and the impulsive heating of the solar corona. Previous solar missions have been limited in sensitivity and dynamic range by the use of indirect imaging, but technological advances now make direct focusing accessible in the HXR regime, and the FOXSI rocket experiment optimizes HXR focusing telescopes for the unique scientific requirements of the Sun. FOXSI has completed three successful flights between 2012 and 2018. This paper gives a brief overview of the experiment, focusing on the third flight of the instrument on 2018 Sept. 7. We present the telescope upgrades highlighting our work to understand and reduce the effects of singly reflected X-rays and show early science results obtained during FOXSI's third flight.

Keywords: The Sun, high-energy, X-rays, sounding rocket, X-ray focusing optics

# 1. INTRODUCTION

The high-energy nature of the Sun remains an important subject of research and challenges our understanding of solar and stellar physics. How the Sun efficiently accelerates particles during solar flares, and how the solar corona gets heated to millions of degrees, remain open and debated questions. X-ray observations of the solar corona provide one of the most direct diagnostic of heating and acceleration of energetic electrons. X-ray bremsstrahlung emission in the solar atmosphere arises from the interaction of energetic electrons with the ambient solar plasma, and its intensity is directly proportional to the density of the ambient medium. As energetic electrons accelerated

Further author information: (Send correspondence to S.M.) S.M.: E-mail: smusset@umn.edu, Telephone: 1 612 625 4518

in the solar corona precipitate along magnetic field lines towards the lower solar atmosphere, the ambient density increases a few orders of magnitude, resulting in intense radiation from the footpoints of coronal structures, and fainter radiation from the particle acceleration sites in the corona. One of the challenges of solar X-ray observations is thus to obtain good sensitivity and dynamic range to be able to characterise energetic electron distributions in the corona, at or close to the sites of energy release, in order to understand where, when and how magnetic energy is converted to heating and particle acceleration in the solar corona.

Imaging and spectroscopy of solar X-ray radiation are challenging measurements: in the hard X-ray domain (HXR,  $\gtrsim 10$  keV), classical telescopes cannot focus the X-ray fluxes. Past solar-dedicated hard X-ray telescopes, such as the Reuven Ramaty High Energy Solar Spectroscopic Imager (RHESSI)<sup>1</sup> were equipped with indirect, Fourier-based imaging systems. On RHESSI, the imaging system used rotating collimators composed of pairs of grids in front of detectors. The modulated signal was reconstructed using Fourier techniques.<sup>2</sup> The Solar Telescope for Imaging X-rays (STIX), which will be launched in 2020 onboard Solar Orbiter, also has an indirect imaging system based on the modulation of the photon flux through pairs of grids to produce moire patterns on the detectors, enabling the measurement of complex visibilities.<sup>3</sup> These indirect imaging methods have limited dynamic range capabilities. Direct imaging of hard X-rays via grazing incidence optics provides an alternative with a dynamic range improved by a least one order of magnitude for solar flare observations.

Hard X-ray observations of the Sun with focusing optics has been performed with the Nuclear Spectroscopic Telescope Array (NuSTAR),<sup>4</sup> launched in 2012. This astrophysical mission is composed of two focusing X-ray telescopes sensitive to the energy range 3-79 keV. The quiet Sun and quiescent active regions have been observed during solar campaigns with NuSTAR,<sup>5,6</sup> however, this mission is not designed for solar observations and solar campaigns are limited to periods of low solar activity to avoid high photon rates. During these campaigns, small scale coronal heating events<sup>7,8</sup> and microflares<sup>9,10</sup> have been observed, and even in the case of small flaring events (GOES class A and below), the NuSTAR observations of solar microflares suffer a high deadtime limiting the capability to observe high-energy photons, the photon flux being dominated by low energy photons. In addition, NuSTAR observations can be contaminated by singly reflected photons (ghost rays) reaching the focal plane, unfocused, by a single reflection in the optics (where two reflections are needed to focus photons).

The FOXSI rocket experiment has been designed to demonstrate the capabilities of focusing optics for solar observations. The instrument has successfully flown three times, in 2012, 2014, and 2018. This paper focuses on the upgrades and early results of the third flight. The instrument design and the previous flight campaigns are summarized in section 2.1 and upgrades for FOXSI-3 are detailed in section 2.2. A description of ghost ray pattern reduction for FOXSI-3 is presented in section 3. Finally, the FOXSI-3 flight and its early results are presented in section 4.

# 2. THE FOCUSING OPTICS X-RAY SOLAR IMAGER (FOXSI) ROCKET EXPERIMENT

# 2.1 The FOXSI rocket campaigns

The FOXSI sounding rocket experiment is composed of seven optic modules paired with seven high-sensitivity semiconductor hard X-ray detectors. <sup>11-13</sup> Each optic module is composed of several nested replicated nickel HXR focusing optics produced at NASA/Marshall Space Flight Center (MSFC). The semiconductor detectors are silicon and cadmium telluride (CdTe) double-sided strip detectors provided by JAXA's Institute of Space and Astronautical Science (ISAS) and Kavli Institute for the Physics and Mathematics of the Universe (IPMU) at the University of Tokyo. <sup>14,15</sup> The focal length of the experiment is 2 meters, and each of the detectors has a field of view that covers roughly a quarter of the solar disk. The focal length of the experiment is limited by the space available on the sounding rocket for the scientific payload, and this limitation in length in return limits the optics grazing angles and thus the high energies that can be observed with the experiment: the FOXSI rocket is optimized for observations in the 4-20 keV energy range. The semiconductor detectors need to be cooled to temperatures below -10°C for optimal performances. On the FOXSI rocket experiment, they are cooled prior to the launch using a controlled flow of liquid nitrogen. A sounding rocket flight provides the opportunity to perform observations during 6 to 7 minutes, before the payload re-enters the atmosphere on its descent back to the ground, where it is recovered. During these few minutes of observations, different regions of the solar disk are

targeted in order to achieve the flight goals; typically, during a FOXSI flight, four targets are observed. The data are telemetered during the flight, allowing access to images and spectra of the X-ray emission in real-time, which are used to decide when to change targets. The pointing to different targets on the solar disk is assured by the Solar Pointing Altitude Rocket Control System (SPARCS) and can be adjusted during the observations. After the first flight of the FOXSI rocket, a Solar Aspect and Alignment System (SAAS) was added to the experiment to assist in-flight pointing corrections by imaging the full solar disk in visible light.

The FOXSI sounding rocket flew for the first time on November 2, 2012, at 17:55 UT, from the White Sands Missile Range in New Mexico, USA. This first flight provided the first focused of image of solar HXR and is fully described in Krucker et al. (2014).<sup>11</sup> In this first version of the FOXSI experiment (FOXSI-1), each optic module was composed of seven nested layers, and paired with double-sided, 75  $\mu$ m strip silicon detectors.<sup>16</sup> Solar observations were made during 6.5 minutes, and four targets were observed, including multiple active regions and a region of the quiet Sun. During the observation of the final target, FOXSI-1 observed a microflare already in progress.<sup>11</sup> Additionally, FOXSI-1 quiescent active region observations were used in combination with coordinated soft X-ray Hinode observations to constrain the hot plasma emission of one of the regions.<sup>17</sup>

For the second flight (FOXSI-2), two optics modules were upgraded to include 10 mirror shells. The additional shells have a smaller diameter, thus smaller grazing angle, increasing the effective area by  $\sim 20\%$  at 10 keV.  $^{12,18}$  Two silicon detectors were replaced by double-sided, 60  $\mu$ m strip CdTe detectors  $^{16,19,20}$  designed at ISAS, which offer 100% efficiency in the high energy end of the FOXSI rocket energy range (10-20 keV). Finally, a Solar Aspect and Alignment System (SAAS) was added to better coalign the experiment with the sounding rocket's SPARCS pointing system.  $^{12,18}$  The second flight of the FOXSI rocket occurred on December 11 2014 at 19:11 UT, again from the White Sands Missile Range. The observations lasted for 6 minutes and 40 seconds, during which four targets were observed, including on-disk and occulted active regions, and an area of the quiet Sun. During this flight, two microflares were observed. The combination of FOXSI-2 HXR observations and Hinode-XRT SXR observation led to the detection of nanoflare heated plasma in an active region.  $^{21}$  The quiet Sun measurements from FOXSI-2 were contaminated with singly reflected photons from the microflares outside of the field of view of the FOXSI detectors. These singly reflected photons (also called ghost rays) are photons which reflect on only one of the Wolter-I optics segments, instead of reflecting on both segments, but still reach the focal plane, without being focused, creating a pattern on the detector that is described in section 3.1.

Limiting ghost rays was one of the goals of the third flight of the FOXSI rocket experiment, and this paper reports the efforts in characterization and mitigation of the ghost rays for FOXSI-3 (section 3), as well as the early results from the flight (section 4).

# 2.2 FOXSI-3 campaign upgrades

The FOXSI-3 rocket experiment was flown with several hardware upgrades, which are shown in figure 1. Optics were upgraded to obtain better sensitivity by increasing the effective area. New HXR detectors were added to increase sensitivity to high energy photons. Collimators were added in front of the optics to reduce ghost rays. A SXR detector was included to widen the FOXSI energy range towards low energies. The mechanical structure of the focal plane was modified to insure a better thermal design. The SAAS was upgraded to provide shorter exposure images during the flight, and to store the uncompressed data onboard during the duration of the flight.

#### 2.2.1 Optics

The FOXSI optics are monolithic Wolter-I shells produced at MSFC, applying a relatively low-cost electroformed nickel alloy replication (ENAR) process.  $^{22,23}$  These monolithic shells provide intrinsically superior angular resolution as opposed to segmented optics since they do not require individual mirror segments to be aligned to each other to build a Wolter-I shell (as is the case with e.g. NuSTAR). For increased effective area, shells of various radii are coaxially nested together into modules of 7 or 10 mirrors. The averaged resolution of the integrated modules was measured in the laboratory to be  $4.3 \pm 0.6$  arcsec (FWHM) for an on-axis source. The measured averaged half-power diameter (HPD) on-axis is  $27 \pm 1.7$  arcseconds (for more information on the FOXSI optics see Krucker et al,  $2013^{24}$  and Buitrago-Casas et al,  $2017^{23}$ ).

For FOXSI-3, two of the 7-shell optic modules were refabricated to include 10 mirror shells. The additional shells have a smaller diameter, and therefore provide smaller grazing angles, increasing the sensitivity to higher

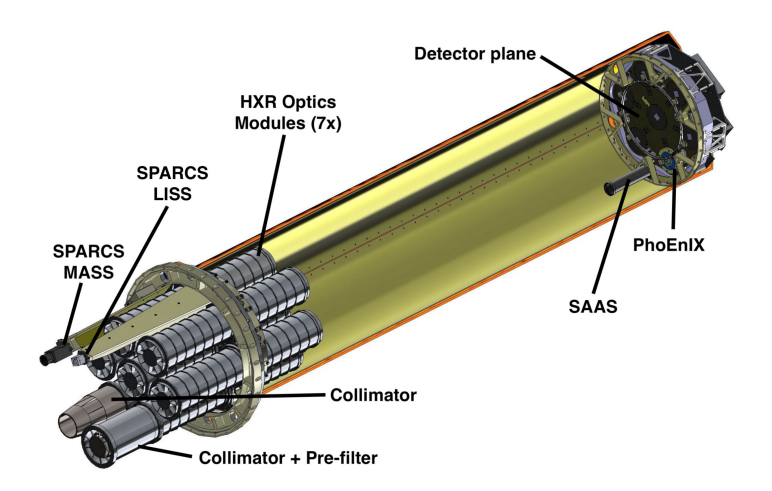


Figure 1. FOXSI-3 payload render. The FOXSI-3 experiment included several upgrades from previous FOXSI instruments. Two additional optics modules were upgraded to include ten nested mirror shells, resulting in four 10-shell modules and three 7-shell modules. Two new CdTe detectors replaced the FOXSI-2 CdTe detectors and a soft X-ray detector (PhoEnIX) replaced a Si detector. Additionally, two honeycomb collimators were included (in front of two optics modules) to eliminate background from ghost rays. The collimator paired with the PhoEnIX detector includes an additional pre-filter.<sup>20</sup>

X-ray energies. The addition of these shells increased the effective area of each module by  $\sim 20\%$  at 10 keV and a factor of  $\sim 2$  at 15 keV.<sup>12</sup>

#### 2.2.2 HXR Detectors

The FOXSI-3 rocket flew four of the original silicon detectors, and two new CdTe detectors fabricated by ACRORAD in Japan, developed and tested JAXA/ISAS and the Kavli IPMU. These CdTe double-sided strip detectors had a similar dimensions as the CdTe detectors used for FOXSI-2, except for the thickness which was increased from 500  $\mu$ m to 750  $\mu$ m:<sup>20</sup> 128 60  $\mu$ m-pitch strips on each side of the detector. These detectors provided a 100% efficiency in high energy end of the FOXSI rocket energy range (10-20 keV), providing a greater sensitivity of the experiment towards high energies. Initial testing of these detectors shows an energy resolution (FWHM) of 0.8 keV at 13.9 keV.<sup>25</sup> The readout of the detectors is performed by four low-noise and low-power-consumption ASICs.<sup>25</sup> To avoid potential noise contamination during the flight, the low-energy threshold chosen for these CdTe detectors (~5-6 keV) was higher than the threshold used for Silicon detectors.<sup>20</sup> Both sides of the detector are bonded to their electronic board using a stud bump bonding technique.<sup>25,26</sup> These bonds can be damaged by rapid temperature changes, therefore, the cooling of the detector was kept at a rate lower than 10°C/hour. For the FOXSI-3 flight, the cooling of the experiment started 7 hours before launch, to reach a temperature below -25°C on the detector boards at launch time, with the detectors powered during the cooling procedure.

#### 2.2.3 SXR detector

For the FOXSI-3 flight, a high-speed back-illuminated Complementary Metal Oxide Semiconductor (CMOS) sensor was added to provide photon-counting imaging-spectroscopy in the soft X-ray range. The Photon Energy Imager in X-rays (PhoEnIX) was a delivered system by the National Astronomical Observatory of Japan (NAOJ) and Nagoya University. The detector is an array composed of 11  $\mu$ m pixels; with the FOXSI focal length of 2 meters, the pixel size corresponds to about 1 arcsecond. The PhoEnIX detector is sensitive in the 0.5-5 keV range, expanding the energy range of the whole FOXSI rocket experiment. In this energy range, high-speed photon-counting is required to read the energy of each single photon. The highest utilized frame rate for the PhoEnIX sensor is 500 fps.<sup>27</sup> The amount of data generated during the flight was to large for the telemetry stream, and most of the data was stored on board during the flight. During the FOXSI-3 flight, two observation modes were used for the PhoEnIX detector. In the slow mode, data was collected on the whole sensor (FOV

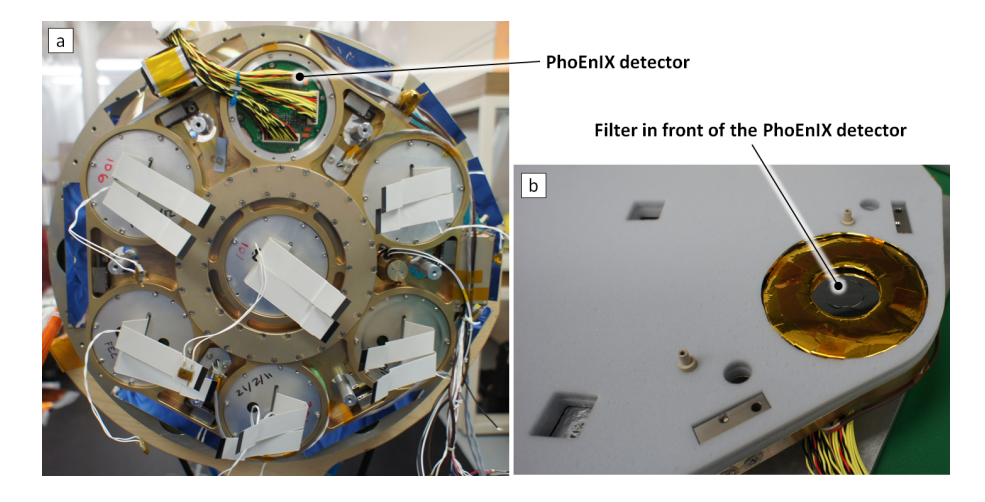


Figure 2. PhoEnIX detector in the FOXSI rocket focal plane. a: back of the focal plane: the extent of connection cables for the PhoEnIX detector prevent from closing the detector housing as it is for other detectors. The need for space on top of PhoEnIX lead to one layer less of thermally insulating foam. b: foam blanket in front of the focal plane. While only small squared windows are needed for HXR detectors, the PhoEnIX detector has a bigger window and a filter in front of the sensor, reducing the amount of foam in that area.

of 19.4 × 36.3 arcmin) at a rate of 4.5 fps. The data collected was stored onboard. In the fast mode, data was collected only in the middle part of the sensor (FOV 19.4 × 7.3 arcmin) at a rate of 253 fps.<sup>20</sup> The data collected in the slow mode was stored on board and the highest-value pixels were included in the telemetry stream to provide information on the X-ray sources seen during the flight. The integration of the PhoEnIX detector into the FOXSI rocket experiment triggered several modifications of the scientific payload. The electronic box associated with PhoEnIX was added on top of the electronic stack behind the focal plane containing the detector. A pre-filter (aluminum coating on a thin polyimide film) was added in front of the optic module associated with the PhoEnIX detector, as well as a filter in front of the detector itself, in order to prevent visible photons to reach the detector. These adjustments resulted in some alteration of the thermal blanketing around the PhoEnIX detector in the focal plane, as seen in figure 2.

### 2.2.4 Thermal design

The detector cooling is assured by a flow of liquid nitrogen in a focal plane plate in which the seven detectors are hold, as seen in panel a of figure 2. This plate is attached at the end of the experiment tube, at the focal plane of the telescopes. In the original design of the FOXSI mechanical structure of the focal plane, the focal plane plate was mounted on the metering tube via fiberglass posts. When cooling from room temperature to -40°C, the focal plane experienced thermal contraction and shrank by about 16 mm in diameter. This caused a  $\sim$ 2 arcminutes misalignment in the SAAS lens tube axis. The design was modified for FOXSI-3. A circular array of titanium flexures provided adequate lateral stiffness and circumferential compliance. These flexures decouple the shrinkage of the focal plane from the SAAS mounting surface. The SAAS tube axis misalignment was expected to be reduced to 0.378 arcseconds. The design and photos of these flexures are shown in figure 3. Measurements during the FOXSI-3 launch campaigns demonstrated that the SAAS alignment was now independent of the focal plane temperature and that the misalignment of the SAAS tube with the experiment was of about 0.1 arcsec.

Another modification of the thermal design was necessary to include the PhoEnIX detector assembly. Due to the height of the PhoEnIX detector board, the thickness of the thermal blanketing was reduced between the back side of the detector board and the first electronic board to ensure that no mechanical constraint was added on the electronic board and connections. Moreover, the PhoEnIX detector array being wider than the HXR detectors, the window in front of the detector had to be widened, resulting in less thermal blanketing in front of this particular detector.

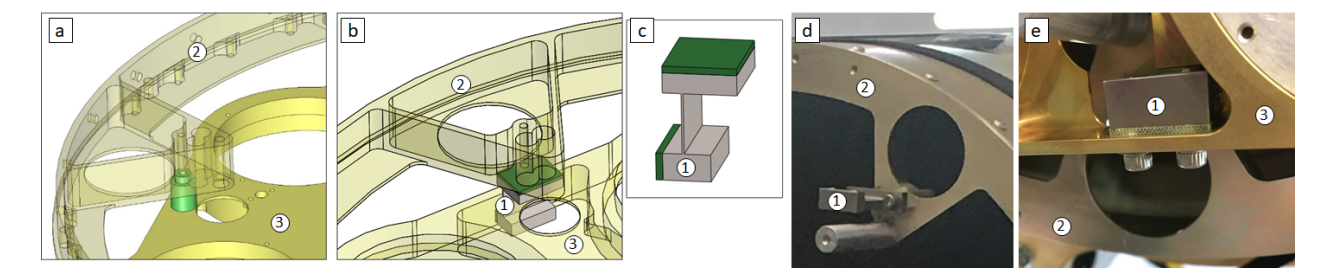


Figure 3. Focal plane mounting (1) between the end of the instrument tube (2) and the focal plane plate (3). a: original fiberglass posts. b: new flexures between the end of the tube and the focal plane, designed to decouple the skrinkage of the focal plane from the end of the tube where the SAAS is mounted. c: design of the flexures: titanium parts are in grey, fiberclass is in green. d: Flexures on the end of the tube, before mounting the focal plane plate. e: End of flexure screwed to the focal plane plate on top of the end of the experiment tube.

# 2.2.5 Solar Aspect and Alignment System

In addition to its X-ray telescopes, FOXSI-3 flew an optical, named the Solar Aspect and Alignment System (SAAS). It consisted of a co-boresighted optical telescope physically coupled to both the optics and detector planes. The purpose of the SAAS was to:

- Establish the alignment offset between the X-ray telescopes and the primary solar aspect system (SPARCS) both before and after launch;
- Provide real-time optical confirmation of pointing during flight;
- Provide a confirmatory record of pointing to assist post-flight analysis.

The primary solar aspect system for FOXSI-3 was the NASA-provided Solar Pointing Attitude Rocket Control System (SPARCS). It is a three-axis solar pointing control system comprised of a coarse (CSS), intermediate (MASS), and fine Sun sensor (LISS). SPARCS employs a pneumatic system and ring laser gyros to achieve a pointing accuracy of 30 arcsec in pitch and yaw and 1.2 degrees in roll with a pointing stability of 0.12 arcsec. However, the alignment between SPARCS and the X-ray telescopes could not be directly established on the ground. Instead SAAS acted as a reference point during both the X-ray and SPARCS alignment procedures during which the offset to SAAS was calculated. From these measurements the offset between SPARCS LISS and the X-ray telescopes was calculated and a correction inserted to the flight pointing control software.

The FOXSI-2 SAAS requirements, design and hardware <sup>18</sup> were reused for FOXSI-3 with the following upgrades:

- The SAAS onboard control computer was upgraded to an Advantech PCM-3365 with 64 GB of onboard Flash storage. This enabled the SAAS to store all full resolution images onboard for post-flight analysis. (The FOXSI-3 SAAS cadence was ~5 frames per second.) The SAAS data telemetered during flight was highly compressed which meant that full resolution could not be achieved without onboard storage.
- Flexures were applied to the mounting of the SAAS camera to the detector bench. This was to remove a temperature dependency on alignment revealed the during the FOXSI-2 campaign. Laser alignment measurements during detector cooling confirm that the flexures successfully removed this behavior.
- A lesser degree of neutral density attenuation was used. (FOXSI-2 used a combination of ND 4.0, ND 0.6 and ND 0.3 filters while FOXSI-3 only used ND 4.0 and ND 0.3.) This enabled shorter exposure times and minimized any potential blurring of images due to spacecraft motion.

In addition to the hardware upgrades, the SAAS pre-flight focusing procedure was altered to utilize WSMRs new heliostat which was not available during the FOXSI-2 campaign. The procedure was performed as close to solar noon as possible to minimize seeing effects due to the Earths atmosphere. Spacers were placed on the screw threads connecting the camera lens to the rest to camera in order to adjust the distance between the lens and the CCD. The optimal distance was chosen based on visual inspection of sunspots observed by the SAAS via the heliostat. This technique eliminated the difficulties caused by poor seeing and non-parallel light rays experienced during the FOXSI-2 campaign when focus was judged by observing the nearby mountain range. This lead to an





Figure 4. Photographs of the optic end of the FOXSI-3 instrument before the launch (left) and close-up on the honeycomb collimator (right). Two honeycomb collimators (2) have been added on top of two of the optic modules (1). Front blockers have been added in front of the remaining optic modules (3).

estimated FOXSI-2 SAAS angular resolution of  $\sim$ 20 arcsec. Although the resolution of the FOXSI-3 SAAS has not yet been confirmed, it was nonetheless an improvement over FOXSI-2.

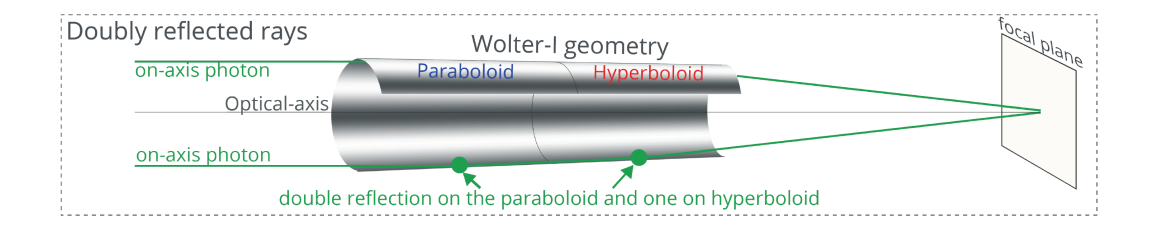
#### 2.2.6 Ghost ray reduction

One of the goals of the FOXSI-3 technical development is to demonstrate technology capable of blocking part of the ghost rays discussed in section 2.1. Different options were considered for FOXSI-3, including cylindrical baffles, honeycomb collimators, and wedge absorbers. <sup>20,23</sup> Two options were finally implemented: a 3D-printed honeycomb collimator and front blockers. Both can be seen in front of the optics of figure 4.

Honeycomb collimators are structures full of parallel cylindrical holes (channels) placed in front of the optic modules for light to travel through.  $^{20,23}$  The aspect ratio controlled by the length and diameter of the channels is optimized to block photons arriving at an angle greater than the desired threshold. In the case of the FOXSI rocket, we choose to block photons with incidence angles greater than 18 arcminutes. The titanium 3D-printed collimators used during the FOXSI-3 flight were fabricated by the Japanese company TORAY Precision Co., Ltd.\*. With this technique, a channel equivalent diameter of 1mm was achieved (in this design channels have a hexagonal shape). The final collimator parameters were optimized to block ghost rays on the four most inner channels of the 7-shell optic module, leading to channel maximal length of 19.5 centimeters. The measured effective area of the collimator is  $\sim 40\%$ ,  $^{20,23}$  leading to a decrease of  $\sim 20\%$  of the module effective area. Two of these collimators were added on the FOXSI-3 payload, as visible in figure 4: one collimator was paired with the soft X-ray detector PhoEnIX, and the second collimator was paired with a silicon detector.

Front and rear blockers are 1.5 mm-thick disks of aluminum placed at both ends of the optic modules in order to reduce the ghost ray patterns. The ideal diameters of the blockers are the result of a trade-off between the reduction of the ghost ray pattern and the vignetting effect on the resulting images. The diameters of the blockers in FOXSI-3 were 3.10 cm for the 10-shell modules and 3.75 cm for the 7-shell modules for the front blockers, and 2.62 and 3.14 cm for the respective rear blockers. Front blockers are visible at the end of the optic modules on figure 4.

The implementation and testing of both the collimator and blockers are described in the next section.





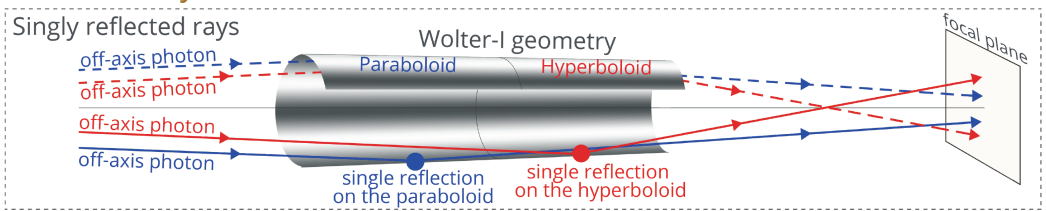


Figure 5. Ghost ray formation on Wolter-I optics. Top panel: doubly reflected rays reflects on the paraboloid and hyberboloid sections of the Wolter-I optics and are focused on the focal plane. Bottom panels: ghost rays are singly reflected rays that reflect on only one of the sections of the Wolter-I optics and reach the focal plane without being focused.

# 3. GHOST RAY ANALYSIS AND REDUCTION FOR FOXSI-3

# 3.1 Ghost rays in focusing optics

FOXSI uses Wolter-I figured grazing incidence X-ray telescopes to focus solar HXRs. The Wolter-I geometry consists of a combination of a paraboloid primary followed by a hyperboloid secondary. In these telescopes, a genuine image is composed of X-rays reflected on both mirrors before impinging the focal plane. A limitation of this type of optics is the stray light, also known as ghost rays. This happens when unreflected or singly reflected HXRs reach the focal plane (Figure 5). Ghost rays are highly dependent on the incident angle; the smaller it is, the closer the stray light to the optical axis.

Ghost rays are typically less of an issue for astrophysical (non-solar) sources, since they often are point sources and are well separated. For these objects where X-ray sources are far enough apart, the effect of stray light can often (though not always) be neglected. However, for extended X-ray sources, as are found on the Sun, ghost rays may severely deteriorate the overall performance of the observations by providing large, uneven backgrounds. Previous space-based astrophysics-dedicated missions using several concentric Wolter-I mirrors have controlled ghost rays by nesting the mirrors together as close as physically possible, or by adding concentric circular sieves at the telescope aperture.

#### 3.2 Ghost ray analysis

The ghost ray patterns can be studied by measuring the point-spread function (PSF) of the FOXSI modules for different off-axis angles of an X-ray sources. Such laboratory measurements were performed at the 100-meter long Stray Light Facility (SLF) at MSFC. An example of this measurement for a sources located 30 arcmin off-axis of a FOXSI 10-shell module is shown in the left panel of figure 6. The experimental setup and several measurements with a 7-shell FOXSI module are presented in Buitrago-Casas et al (2017).<sup>23</sup>

In order to investigate numerically the ghost ray patterns and the options to reduce the ghost ray contamination of the FOXSI field of view, a Monte Carlo ray-tracing simulation was developed, following the method described in Elsner et al.<sup>28</sup> The simulation is described in Buitrago-Casas et al (2017).<sup>23</sup> One particularity of the simulation is that the history of each of the simulated ray is tracked, so that it is possible to determine on which part of the Wolter-I optics the ray was reflected. The results of the ray-tracing simulation for a source

<sup>\*</sup>https://www.tpc.toray/en/

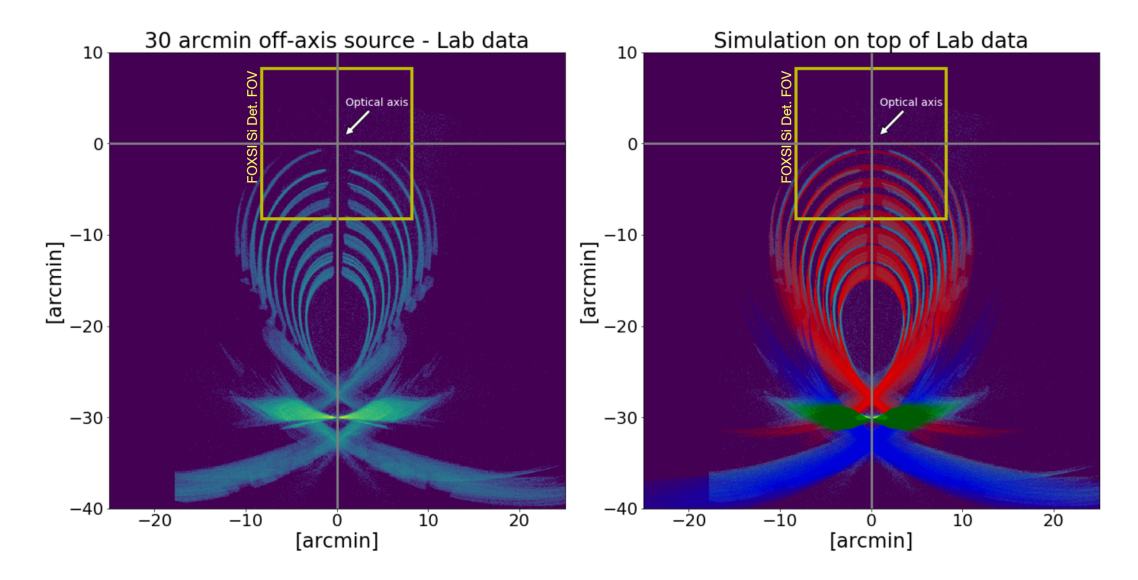


Figure 6. Left panel: lab measurement of the ghost ray pattern at MSFC. Right panel: ray-tracing simulation superimposed on the lab measurement. Ghost rays reflected on the paraboloid section of the optics are shown in blue; ghost rays reflection on the hyperboloid section are shown in red, and focused rays doubly reflected are shown in green. In both figures, the field of view of a FOXSI silison detector is shown for reference. The source is located 30 arcminutes from the detector optical axis.

located 30 arcmin off axis a FOXSI 10-shell optic module is shown on the right panel of figure 6, superimposed on the corresponding lab measurement. As it can be seen on figure 6, the ray-tracing simulation recovers all of the features that have been measured in the Stray Light Facility, and provides information on the origin of the ghost ray patterns.

This ray-tracing simulation tools was therefore used to investigate possible solutions to reduce the ghost ray contamination for the FOXSI-3 flight. In the following section, we will describe the two options that were implemented on FOXSI-3: a honeycomb collimator and front blockers.

### 3.3 Ghost ray reduction for the FOXSI-3 flight

As described in section 2.2.6, the two options implemented to reduce the ghost ray pattern during the FOXSI-3 flight were a honeycomb collimator and front blockers in front of the optic modules. In order to characterized their effectiveness to block some of the ghost rays, lab measurements were performed at the Stray Light Facility at MSFC. The PSF of an X-ray source located at a distance of 100 meters from the FOXSI focal plane, and with an incidence angle of 30 arcmin, was measured for a 7-shell optic module, without any ghost ray blocking device, with the honeycomb collimator, and with a front blocker of 3.10 cm-diameter. The results of these measurements are visible in figure 7.

The left panel of figure 7 shows the effect of the honeycomb collimator on the ghost ray pattern. As described in section 2.2.6, this collimator was designed to stop ghost rays reflecting on the four inner most optics of the 7-shell optic module. On the measurement, one can clearly see that ghost rays from the four larger inner curves of the pattern have been blocked. Furthermore, ghost rays have been eliminated in other parts of the pattern.

The right panel of figure 7 show the effect of the optimized blockers on the ghost ray pattern. The ray-tracing simulations showed that blockers would eliminate ghost rays induced front one reflection on the paraboloid section of the Wolter-I configuration. As shown in figure 6, X-rays reflecting once on the paraboloid section of the optics contribute to the outer curve and wings on the ghost ray pattern. On the right panel of 7, one can indeed see that most of the ghost rays in these part of the pattern disappear when the blocker is present.

The honeycomb collimator and the blockers can be combined in the same optic module, and when combined, they eliminate all ghost rays in the FOXSI field of view, shown by the blue box in figure 7. Such combination

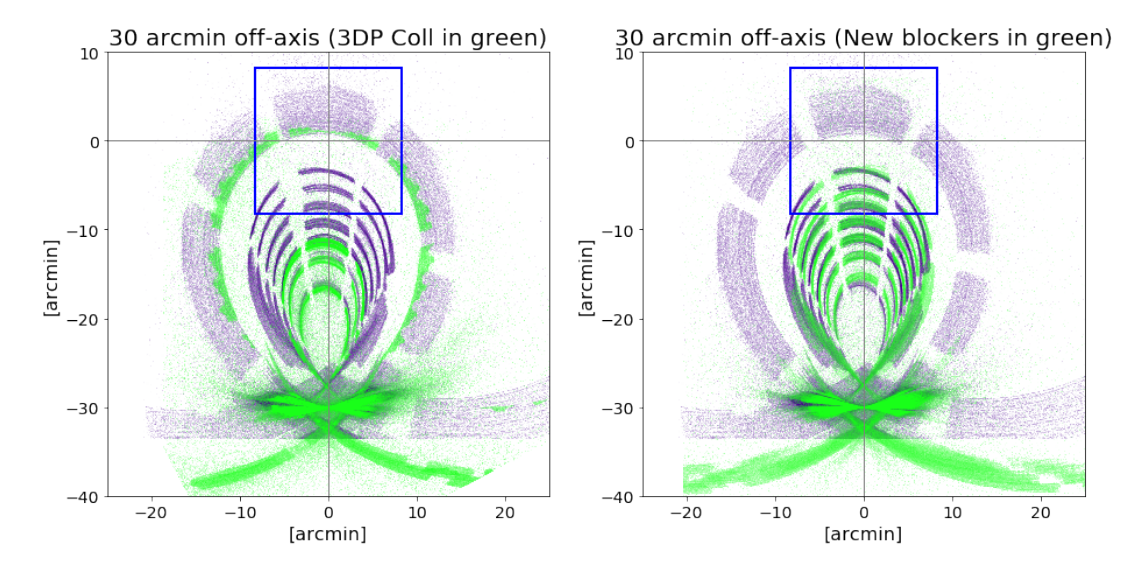


Figure 7. Lab measurement of the ghost ray pattern at MSFC, for a source located 30 arcminutes off-axis of a 10-shell FOXSI optic module. In each panel, the blue pattern is the ghost ray pattern obtained without any ghost ray limitating device. The green patterns are the ghost ray patterns obtained with either a collimator (left panel) or a blocker (right panel) in front of the optics. When a front blocker and a collimator are combined in front of an optic module, all ghost rays are eliminated from the FOXSI detector field of view (shown as a blue square on both panels).

was used on the optic modules paired with the PhoEnIX detector and one silicon HXR detector for the FOXSI-3 flight.

# 4. FOXSI-3 FLIGHT

The scientific questions targeted by the third flight of the FOXSI sounding rocket are the following: Do small impulsive energy releases significantly heat active regions? Do flares occur in the quiet Sun? The objectives of the flight were to increase the number of active regions observed by the FOXSI sounding rocket, in particular with an increased sensitivity to high temperatures, and to place a more stringent upper limit on the quiet Sun emission in hard X-ray.

The launch campaign for FOXSI-3 corresponds to a time of very low solar activity. On the day of the FOXSI-3 flight, an aged active region was visible on the disk, with very low probability of flaring activity. A coronal hole was identified at the north pole of the Sun. Small brightenings in AIA hot channels were observed outside of the active region before the launch. The FOXSI observation plan included to target the active region, the north pole, and a portion of the quiet Sun inclusing off-limb observations on the east side of the Sun. The south pole was an optional target in the case of no obvious source of X-ray emission was observed in the three targets mentioned. An estimate of the active region HXR emission from AIA observations prior to the flight indicated marginal, if any, detection in FOXSI-3 HXR.

# 4.1 Description of the flight

The FOXSI-3 flight took place from the White Sands Missile Range on September 7, 2018, at 17:21 UT. The rocket reached the altitude of 300 km. Observations were carried out for 6.1 minutes. Three targets were observed: an aging active region (target 1), the north pole, with a coronal hole boundary (target 2), and a portion of the quiet Sun including off-limb observations (target 3). The first target was again observed at the end (target 4) of the flight, and finally a slight shift in position was applied to catch a brightening near the west solar limb (target 5). The pointing details of the flight are described in table 1 and an approximate field of view of each target in shown in figure 8. The pointing accuracy (for pitch and yaw) for the SPARCS was better than 1 arcsec during the observations. The roll angle of the payload was slowly drifting during the flight, and this

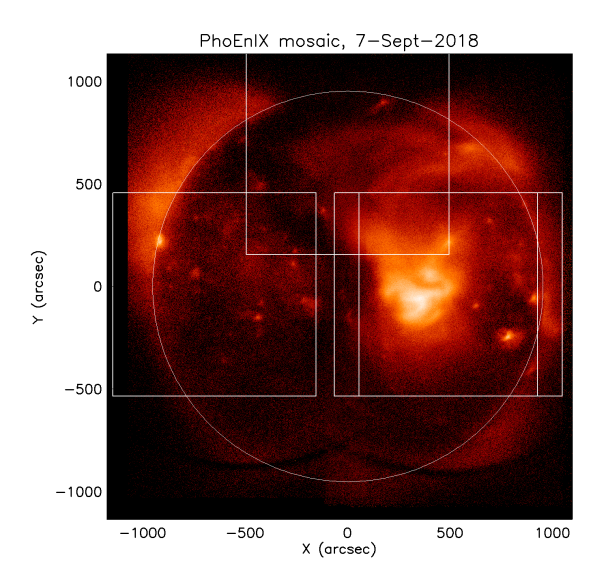


Figure 8. Targets during the FOXSI-3 flight: each white rectangle represents the field of view of a silicon detector on FOXSI-3 for each of the targets. The background image is a mosaic of images from the PhoEnIX sensor onboard FOXSI-3, showing SXR emission between 0.5 and 2 keV.

Target number	Position (arcsec)	Integration time
1	+429.9", -39.6"	$128.2  \sec$
2	-0.2", +650.7"	$24.0  \sec$
3	-650.7", -39.6"	$144.6  \sec$
4	+429.8", -39.6"	$26.3  \sec$
5	+550.7", -39.6"	$44.2  \sec$

Table 1. Position and integration times for the different targets during the FOXSI-3 flight.

will be corrected in the data reduction. The SAAS successfully telemetered and recorded full-Sun data in the visible range during the flight.

Before the flight, the detectors were cooled to a temperature between -20 and -25°C. The 5 temperature sensors located on detector boards showed increases of temperature ranging from 4 to 10°C during the whole flight, and all measured temperatures stayed below -14°C during the observation time range, as shown in figure 9. Data was successfully acquired in all 6 hard X-ray detectors and the PhoEnIX soft X-ray detector.

# 4.2 Coordinated observations

The FOXSI-3 flight observations were coordinated with other solar and astrophysical observatories. Coordinated observations of the active region were obtained with NuSTAR, the X-Ray Telescope (XRT) and the EUV Imaging Spectrometer (EIS) onboard Hinode, and the Interface Region Imaging Spectrograph (IRIS). Images of the full Sun were also obtained with Hinode/XRT before and after the FOXSI flight, and with Atmospheric Imaging Assembly (AIA) onboard the Solar Dynamic Observatory (SDO). Ground-based radio observations were also coordinated with the Expanded Owens Valley Solar Array (EOVSA), the Long Wvelength Array (LWA) and the Solar Submillimeter Telescope (SST).

The IRIS coordinated observations with FOXSI-3 include scans of the quiet sun target before the launch, and of the active region before, during and after the FOXSI-3 flight. Data types are summarized in table 2. During the flight, rapid repeated scans of the active regions were performed with two filters, while before and after the flight, single scans were performed in four different filters.

The EIS coordinate observations with FOXSI-3 also included scans of the active regions and one scan of the quiet Sun region observed by FOXSI. Table 3 summarize the different observations performed.

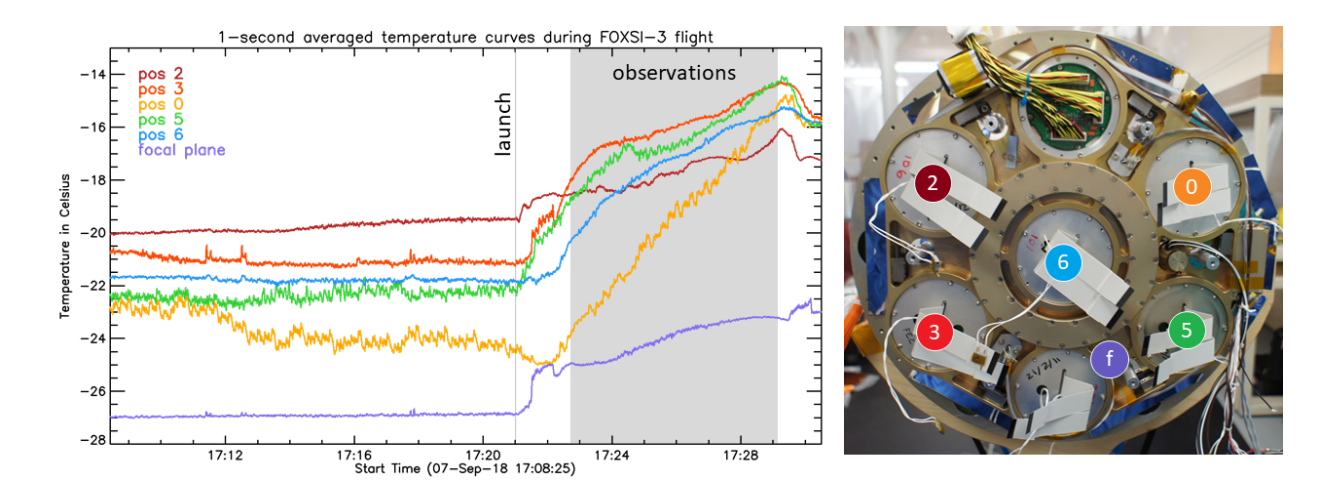


Figure 9. Evolution of temperatures measured on detector boards and on the focal plane plate during the FOXSI-3 flight. Left: Time evolution of different measured temperatures in the focal plane. The vertical line indicates launch time, when the cooler disconnects from the payload. The grey area show the observation time range. Right: position of the different sensors in the focal plane. Five sensors were located on the detector boards inside the detector housing. The last sensor (f) was located on the focal plane plate.

Time	Target	FOV center	Raster type	SJI Filters
14:44 to 15:06	Quiet Sun (single scan)	-673", +45"	256-step	1330, 1400, 2796, 2832
15:46 to 16:05	Active Region (single scan)	+161", -56"	320-step	1330, 1400, 2796, 2832
16:15 to 17:04	Active Region (single scan)	+267", -57"	320-step	1330, 1400, 2796, 2832
17:14 to 18:25	Active Region (repeated scans)	+243", -57"	16-step	1400, 2796
18:35 to 19:24	Active Region (single scan)	+255", -58"	320-step	1330, 1400, 2796, 2832

Table 2. Summary of the IRIS coordinated observations for FOXSI-3

The XRT telescope was scanning the active region during the FOXSI-3 flight. Multiple images were taken in two filters: Be\_thin/Open and Al\_poly/Open. Automatic exposure control was used the exposure time was 16.4s for Be\_thin/Open, and 11.6 and 20.5 seconds for Al\_poly/Open. The full field of view was of  $256" \times 256"$  centered to (+440", -14.5").

#### 4.3 Early results from FOXSI-3

Photon-counting imaging spectroscopy in SXR has not been previously available for solar observations, as fast readout systems are required. Instead, SXR diagnostics usually relies on imaging in different filters, providing some temperature information using ratios of intensities in different wavelengths.

Recent technological development of CMOS sensors enabled this technology and the PhoEnIX detector provided the first photon-counting imaging and spectroscopy during the FOXSI-3 flight, providing spectral information in the various regions imaged. An overview of the photon-counting process with PhoEnIX is illustrated in figure 10.

The PhoEnIX array being larger that the HXR detector arrays, it was possible to reconstruct a full Sun image of the SXR emission during the FOXSI-3 flight using a mosaic of the PhoEnIX observations. This mosaic is shown in figure 8.

Solar activity being very low at the moment of the FOXSI-3 flight, the HXR signal is very weak. Data has been successfully acquired in all HXR detectors, and the ongoing analysis aims to determine if the signal seen in the detector is entirely due to background emission or if some solar component is present in the registered count flux.

	Time	Target	Type of observation	Number of scans
ĺ	06:53 to 11:10	Active Region	Large FOV deep raster	3
	11:15 to 12:20	Active Region	Full CCD raster	1
	15:25 to 16:28	Active Region	Large FOV deep raster	1
	17:15 to 18:19	Active Region	Small FOV narrow-slit raster	7
İ	18:58 to 20:01	Quiet Sun	Large FOV deep raster	1

Table 3. Summary of the EIS coordinated observations for FOXSI-3

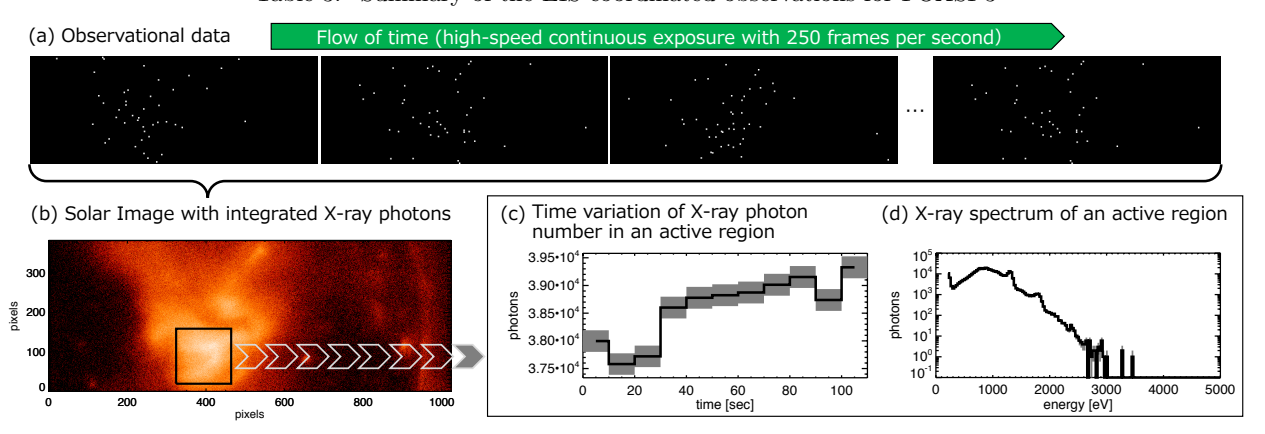


Figure 10. Photon-counting data aquisition in SXR during the FOXSI-3 flight with the PhoEnIX sensor. (a) The photon time of arrival, position and energy are registered for each individual photon arriving on the sensor in one frame time. (b) The integration of the frame observations is used to reconstruct images: here the image of the active region is shown. (c) Since time and energy information are known for each photon, the time evolution and spectrum of a given region in the image can be computed.

### 5. CONCLUSION

The FOXSI sounding rocket experiment successfully demonstrated focusing optics for SXR and HXR solar observations. For FOXSI-3, two options were implemented to reduce the ghost ray pattern and demonstrated in laboratory. During the third flight of the experiment, the first photon-counting imaging spectroscopy of solar SXR emission was performed.

Some of the remaining challenges of the FOXSI rocket experiment include the increase of the spatial resolution of HXR observations, to facilitate the comparison with SXR and EUV observations that achieve arcsec resolution and below. Being able to resolve the smaller scales will undoubtedly provide new insight about the complexity and the characteristics of energy release in the solar corona. Another challenge for a solar-dedicated instrument is the capability to perform high quality observations with high-rate photon fluxes during solar flares. Both those challenges will be addressed in a FOXSI-4 sounding rocket, which will be proposed to LCAS this year. For FOXSI-4, we propose a flare campaign, where FOXSI and other rocket payloads would wait for a flare to happen before launching the rocket(s) to perform flare observations.

One other challenge remaining in focused solar X-ray observations is to observe HXR photons of higher energies. In a sounding rocket, the length of the payload is limited, and the current focal length of the FOXSI rocket experiment (2 meter) cannot be significantly extended. The focal length being a limiting factor in the incidence angles that can be achieve, it is a direct limitation on the high energy limit. However, NuSTAR demonstrated the possibility to use extensive booms to achieve long focal lengths (10 meters on NuSTAR). The next great advances in HXR solar observations could therefore be accomplished with a FOXSI-like instrument on a spacecraft, enabling observations of solar HXR emissions with high sensitivity and high dynamic range, at energies of a few tens of keV.

#### ACKNOWLEDGMENTS

The FOXSI-3 sounding rocket is funded by NASA LCAS grant NNX16AL60G. We acknowledge the NSF for its support of space physics at UMN via a faculty development grant AGS-1429512. The FOXSI team is grateful to the NSROC teams at WSMR and Wallops for the excellent operation of their systems. Furthermore, the authors would like to acknowledge the contributions of each member of the FOXSI experiment team to the project, particularly our team members at ISAS and Kavli IPMU for the provision of Si and CdTe detectors and at MSFC for the fabrication of the focusing optics.

This work was supported by NASA Headquarters under the NASA Earth and Space Science Fellowship Program Grant 80NSSC17K0430.

This work was supported by JSPS KAKENHI Grant Numbers JP17H04832, JP16H02170, JP16H03966, JP24244021, JP20244017, and World Premier International Research Center Initiative (WPI), MEXT, Japan.

This work was supported by JSPS KAKENHI Grant Numbers JP18H03724, JP18H05463, JP17H04832, JP16H02170, JP15H03647, JP21540251.

#### REFERENCES

- [1] Lin, R. P., Dennis, B. R., Hurford, G. J., Smith, D. M., Zehnder, A., Harvey, P. R., Curtis, D. W., Pankow, D., Turin, P., Bester, M., Csillaghy, A., Lewis, M., Madden, N., van Beek, H. F., Appleby, M., Raudorf, T., McTiernan, J., Ramaty, R., Schmahl, E., Schwartz, R., Krucker, S., Abiad, R., Quinn, T., Berg, P., Hashii, M., Sterling, R., Jackson, R., Pratt, R., Campbell, R. D., Malone, D., Landis, D., Barrington-Leigh, C. P., Slassi-Sennou, S., Cork, C., Clark, D., Amato, D., Orwig, L., Boyle, R., Banks, I. S., Shirey, K., Tolbert, A. K., Zarro, D., Snow, F., Thomsen, K., Henneck, R., McHedlishvili, A., Ming, P., Fivian, M., Jordan, J., Wanner, R., Crubb, J., Preble, J., Matranga, M., Benz, A., Hudson, H., Canfield, R. C., Holman, G. D., Crannell, C., Kosugi, T., Emslie, A. G., Vilmer, N., Brown, J. C., Johns-Krull, C., Aschwanden, M., Metcalf, T., and Conway, A., "The Reuven Ramaty High-Energy Solar Spectroscopic Imager (RHESSI)," Solar Physics 210, 3–32 (Nov 2002).
- [2] Hurford, G. J., Schmahl, E. J., Schwartz, R. A., Conway, A. J., Aschwanden, M. J., Csillaghy, A., Dennis, B. R., Johns-Krull, C., Krucker, S., Lin, R. P., McTiernan, J., Metcalf, T. R., Sato, J., and Smith, D. M., "The RHESSI Imaging Concept," Solar Physics 210, 61–86 (Nov 2002).
- [3] Benz, A. O., Krucker, S., Hurford, G. J., Arnold, N. G., Orleanski, P., Gröbelbauer, H. P., Klober, S., Iseli, L., Wiehl, H. J., Csillaghy, A., Etesi, L., Hochmuth, N., Battaglia, M., Bednarzik, M., Resanovic, R., Grimm, O., Viertel, G., Commichau, V., Meuris, A., Limousin, O., Brun, S., Vilmer, N., Skup, K. R., Graczyk, R., Stolarski, M., Michalska, M., Nowosielski, W., Cichocki, A., Mosdorf, M., Seweryn, K., Przepiórka, A., Sylwester, J., Kowalinski, M., Mrozek, T., Podgorski, P., Mann, G., Aurass, H., Popow, E., Onel, H., Dionies, F., Bauer, S., Rendtel, J., Warmuth, A., Woche, M., Plüschke, D., Bittner, W., Paschke, J., Wolker, D., Van Beek, H. F., Farnik, F., Kasparova, J., Veronig, A. M., Kienreich, I. W., Gallagher, P. T., Bloomfield, D. S., Piana, M., Massone, A. M., Dennis, B. R., Schwarz, R. A., and Lin, R. P., "The spectrometer telescope for imaging x-rays on board the Solar Orbiter mission," in [Proceedings of the SPIE], Society of Photo-Optical Instrumentation Engineers (SPIE) Conference Series 8443, 84433L (Sep 2012).
- [4] Harrison, F. A., Craig, W. W., Christensen, F. E., Hailey, C. J., Zhang, W. W., Boggs, S. E., Stern, D., Cook, W. R., Forster, K., Giommi, P., Grefenstette, B. W., Kim, Y., Kitaguchi, T., Koglin, J. E., Madsen, K. K., Mao, P. H., Miyasaka, H., Mori, K., Perri, M., Pivovaroff, M. J., Puccetti, S., Rana, V. R., Westergaard, N. J., Willis, J., Zoglauer, A., An, H., Bachetti, M., Barrière, N. M., Bellm, E. C., Bhalerao, V., Brejnholt, N. F., Fuerst, F., Liebe, C. C., Markwardt, C. B., Nynka, M., Vogel, J. K., Walton, D. J., Wik, D. R., Alexander, D. M., Cominsky, L. R., Hornschemeier, A. E., Hornstrup, A., Kaspi, V. M., Madejski, G. M., Matt, G., Molendi, S., Smith, D. M., Tomsick, J. A., Ajello, M., Ballantyne, D. R., Baloković, M., Barret, D., Bauer, F. E., Blandford, R. D., Brandt, W. N., Brenneman, L. W., Chiang, J., Chakrabarty, D., Chenevez, J., Comastri, A., Dufour, F., Elvis, M., Fabian, A. C., Farrah, D., Fryer, C. L., Gotthelf, E. V., Grindlay, J. E., Helfand, D. J., Krivonos, R., Meier, D. L., Miller, J. M., Natalucci, L., Ogle, P., Ofek, E. O., Ptak, A., Reynolds, S. P., Rigby, J. R., Tagliaferri, G., Thorsett, S. E., Treister, E., and Urry, C. M., "The Nuclear Spectroscopic Telescope Array (NuSTAR) High-energy X-Ray Mission," Astrophysical Journal 770, 103 (Jun 2013).

- [5] Hannah, I. G., Grefenstette, B. W., Smith, D. M., Glesener, L., Krucker, S., Hudson, H. S., Madsen, K. K., Marsh, A., White, S. M., Caspi, A., Shih, A. Y., Harrison, F. A., Stern, D., Boggs, S. E., Christensen, F. E., Craig, W. W., Hailey, C. J., and Zhang, W. W., "The First X-Ray Imaging Spectroscopy of Quiescent Solar Active Regions with NuSTAR," Astrophysical Journal, Letters 820, L14 (Mar 2016).
- [6] Grefenstette, B. W., Glesener, L., Krucker, S., Hudson, H., Hannah, I. G., Smith, D. M., Vogel, J. K., White, S. M., Madsen, K. K., Marsh, A. J., Caspi, A., Chen, B., Shih, A., Kuhar, M., Boggs, S. E., Christensen, F. E., Craig, W. W., Forster, K., Hailey, C. J., Harrison, F. A., Miyasaka, H., Stern, D., and Zhang, W. W., "The First Focused Hard X-ray Images of the Sun with NuSTAR," Astrophysical Journal 826, 20 (Jul 2016).
- [7] Marsh, A. J., Smith, D. M., Glesener, L., Klimchuk, J. A., Bradshaw, S. J., Vievering, J., Hannah, I. G., Christe, S., Ishikawa, S.-n., and Krucker, S., "Hard X-Ray Constraints on Small-scale Coronal Heating Events," *Astrophysical Journal* 864, 5 (Sep 2018).
- [8] Kuhar, M., Krucker, S., Glesener, L., Hannah, I. G., Grefenstette, B. W., Smith, D. M., Hudson, H. S., and White, S. M., "NuSTAR Detection of X-Ray Heating Events in the Quiet Sun," Astrophysical Journal, Letters 856, L32 (Apr 2018).
- [9] Wright, P. J., Hannah, I. G., Grefenstette, B. W., Glesener, L., Krucker, S., Hudson, H. S., Smith, D. M., Marsh, A. J., White, S. M., and Kuhar, M., "Microflare Heating of a Solar Active Region Observed with NuSTAR, Hinode/XRT, and SDO/AIA," Astrophysical Journal 844, 132 (Aug 2017).
- [10] Glesener, L., Krucker, S., Hannah, I. G., Hudson, H., Grefenstette, B. W., White, S. M., Smith, D. M., and Marsh, A. J., "NuSTAR Hard X-Ray Observation of a Sub-A Class Solar Flare," *Astrophysical Journal* 845, 122 (Aug 2017).
- [11] Krucker, S., Christe, S., Glesener, L., Ishikawa, S.-n., Ramsey, B., Takahashi, T., Watanabe, S., Saito, S., Gubarev, M., Kilaru, K., Tajima, H., Tanaka, T., Turin, P., McBride, S., Glaser, D., Fermin, J., White, S., and Lin, R., "First Images from the Focusing Optics X-Ray Solar Imager," Astrophysical Journal, Letters 793, L32 (Oct 2014).
- [12] Glesener, L., Krucker, S., Christe, S., Ishikawa, S.-n., Buitrago-Casas, J. C., Ramsey, B., Gubarev, M., Takahashi, T., Watanabe, S., Takeda, S., Courtade, S., Turin, P., McBride, S., Shourt, V., Hoberman, J., Foster, N., and Vievering, J., "The FOXSI solar sounding rocket campaigns," in [Proceedings of the SPIE], Society of Photo-Optical Instrumentation Engineers (SPIE) Conference Series 9905, 99050E (Jul 2016).
- [13] Glesener, L. E., Faint Coronal Hard X-rays From Accelerated Electrons in Solar Flares, PhD thesis, University of California, Berkeley (Jan 2012).
- [14] Ishikawa, S.-n., Watanabe, S., Fukuyama, T., Sato, G., Kokubun, M., Odaka, H., Saito, S., Takahashi, T., Nakazawa, K., and Tanaka, T., "Development of Double-Sided CdTe Strip Detectors for γ-Ray Imaging and Spectroscopy," Japanese Journal of Applied Physics 49, 116702 (Nov 2010).
- [15] Ishikawa, S., Saito, S., Tajima, H., Tanaka, T., Watanabe, S., Odaka, H., Fukuyama, T., Kokubun, M., Takahashi, T., Terada, Y., Krucker, S., Christe, S., McBride, S., and Glesener, L., "Fine-Pitch Semiconductor Detector for the FOXSI Mission," *IEEE Transactions on Nuclear Science* 58, 2039–2046 (Aug 2011).
- [16] Athiray, P. S., Buitrago-Casas, J. C., Bergstedt, K., Vievering, J., Musset, S., Ishikawa, S.-n., Glesener, L., Takahashi, T., Watanabe, S., Courtade, S., Christe, S., Krucker, S., Goetz, K., and Monson, S., "Calibration of the hard x-ray detectors for the FOXSI solar sounding rocket," in [Proceedings of the SPIE], Society of Photo-Optical Instrumentation Engineers (SPIE) Conference Series 10397, 103970A (Aug 2017).
- [17] Ishikawa, S.-n., Glesener, L., Christe, S., Ishibashi, K., Brooks, D. H., Williams, D. R., Shimojo, M., Sako, N., and Krucker, S., "Constraining hot plasma in a non-flaring solar active region with FOXSI hard X-ray observations," *Publications of the ASJ* 66, S15 (Dec 2014).
- [18] Christe, S., Glesener, L., Buitrago-Casas, J. C., Ishikawa, S.-n., Ramsey, B., Gubarev, M., Kilaru, K., J. Kolodziejczak, J., Watanabe, S., Takahashi, T., Tajima, H., Turin, P., Shourt, V., Foster, N., and Krucker, S., "Foxsi-2: Upgrades of the focusing optics x-ray solar imager for its second flight," *Journal of Astronomical Instrumentation* 05, 1640005 (03 2016).
- [19] Ishikawa, S.-n., Katsuragawa, M., Watanabe, S., Uchida, Y., Takeda, S., Takahashi, T., Saito, S., Glesener, L., Buitrago-Casas, J. C., Krucker, S., and Christe, S., "Fine-pitch CdTe detector for hard X-ray imaging and spectroscopy of the Sun with the FOXSI rocket experiment," *Journal of Geophysical Research (Space Physics)* 121, 6009–6016 (Jul 2016).

- [20] Vievering, J. T., Nature of Energy Release and Transfer for Solar and Stellar Flares Using High-Sensitivity Hard X-ray Instrumentation, PhD thesis, University of Minnesota (2019).
- [21] Ishikawa, S.-n., Glesener, L., Krucker, S., Christe, S., Buitrago-Casas, J. C., Narukage, N., and Vievering, J., "Detection of nanoflare-heated plasma in the solar corona by the FOXSI-2 sounding rocket," *Nature Astronomy* 1, 771–774 (Oct 2017).
- [22] Ramsey, B. D., "The development of focusing optics for the hard-X-ray region," Advances in Space Research 38, 2985–2988 (Jan 2006).
- [23] Buitrago-Casas, J. C., Elsner, R., Glesener, L., Christe, S., Ramsey, B., Courtade, S., Ishikawa, S.-n., Narukage, N., Turin, P., Vievering, J., Athiray, P. S., Musset, S., and Krucker, S., "Methods for reducing singly reflected rays on the Wolter-I focusing mirrors of the FOXSI rocket experiment," in [Proceedings of the SPIE], Society of Photo-Optical Instrumentation Engineers (SPIE) Conference Series 10399, 103990J (Aug 2017).
- [24] Krucker, S., Christe, S., Glesener, L., Ishikawa, S., Ramsey, B., Gubarev, M., Saito, S., Takahashi, T., Watanabe, S., Tajima, H., Tanaka, T., Turin, P., Glaser, D., Fermin, J., and Lin, R. P., "The focusing optics x-ray solar imager (FOXSI): instrument and first flight," in [Proceedings of the SPIE], Society of Photo-Optical Instrumentation Engineers (SPIE) Conference Series 8862, 88620R (Sep 2013).
- [25] Furukawa, K., Buitrago-Casas, J. C., Vievering, J., Hagino, K., Glesener, L., Athiray, P. S., Krucker, S., Watanabe, S., Takeda, S., Ishikawa, S., Musset, S., Christe, S., and Takahashi, T., "Development of 60 μm pitch CdTe double-sided strip detectors for the FOXSI-3 sounding rocket experiment," Nuclear Instruments and Methods in Physics Research A 924, 321–326 (Apr 2019).
- [26] Takahashi, T., Watanabe, S., Kouda, M., Sato, G., Okada, Y., Kubo, S., Kuroda, Y., Onishi, M., and Ohno, R., "High-resolution CdTe detector and applications to imaging devices," *IEEE Transactions on Nuclear Science* 48, 287–291 (Jun 2001).
- [27] Ishikawa, S.-n., Takahashi, T., Watanabe, S., Narukage, N., Miyazaki, S., Orita, T., Takeda, S., Nomachi, M., Fujishiro, I., and Hodoshima, F., "High-speed X-ray imaging spectroscopy system with Zynq SoC for solar observations," Nuclear Instruments and Methods in Physics Research A 912, 191–194 (Dec 2018).
- [28] Elsner, R. F., O'Dell, S. L., Ramsey, B. D., and Weisskopf, M. C., "Methods of optimizing x-ray optical prescriptions for wide-field applications," in [Proceedings of the SPIE], Society of Photo-Optical Instrumentation Engineers (SPIE) Conference Series 7732, 77322L (Jul 2010).
- [29] Winebarger, A., Glesener, L., and Reeves, K., "Solar Flare Sounding Rocket Campaign," tech. rep., White Paper (2019).